Meltwater produced by wind-albedo interaction stored in an East Antarctic ice shelf
Supplementary Information

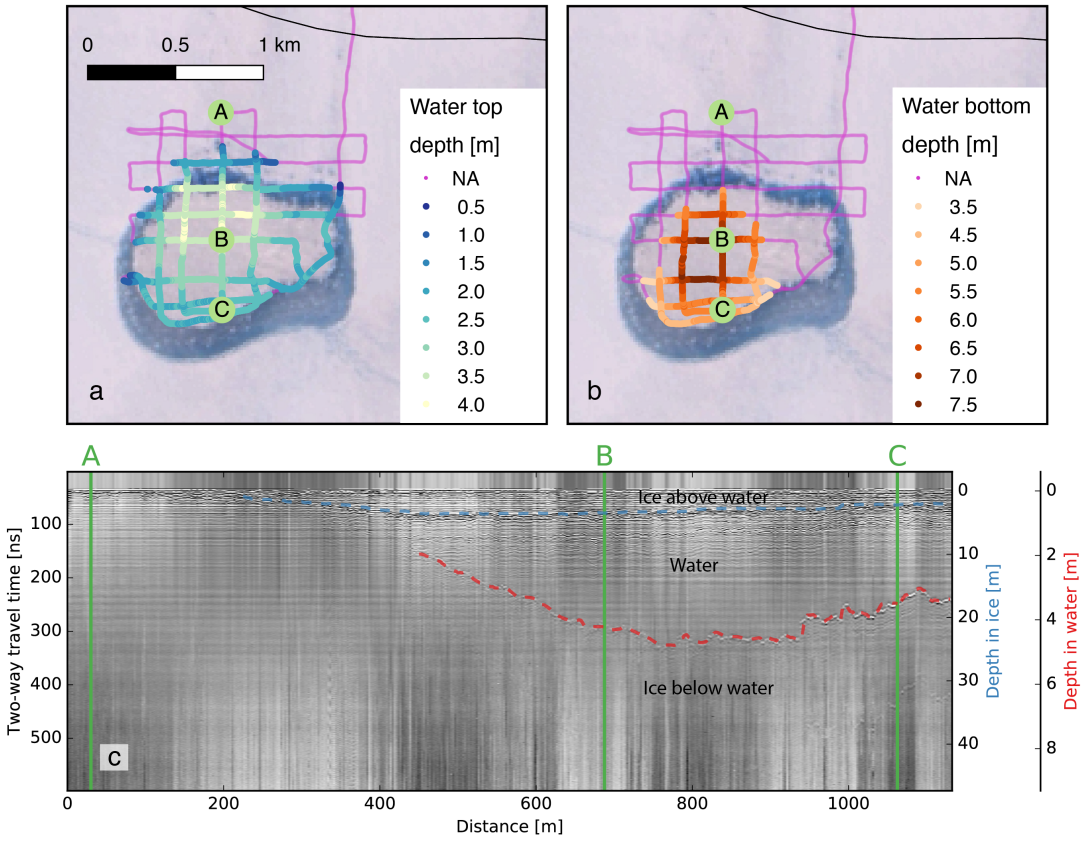

Supplementary Figure 1: **(a)** Upper and **(b)** lower surface of an englacial lake surveyed by radar and drilling (Supplementary Video 2). The radar cross section (c) shows delineation of the upper (blue) and lower boundary (red), with the approximate depths in ice and water shown on the right axis. The travel time-to-depth conversion for radar data across englacial lakes uses a two-layer velocity model: the upper layer is assumed to consist of pure ice (with a radio-wave velocity of $1.68{\cdot}10^8$ m s^{-1}), whereas the lower layer is assumed to be fresh water (with a radio-wave velocity $0.33{\cdot}10^8$ m s^{-1}). Because englacial lakes where found exclusively in blue ice areas with negligible firn cover, assuming the pure ice velocity is justified, although it does not account for a potential inclusion of water bubbles. The latter causes a slower radio-wave velocity (and correspondingly thinner burial depths). However, comparison with ice-core drilling reveals differences smaller than 0.2 m for both layers at the core location, indicating that the radar-inferred depths are accurate to within 5%.

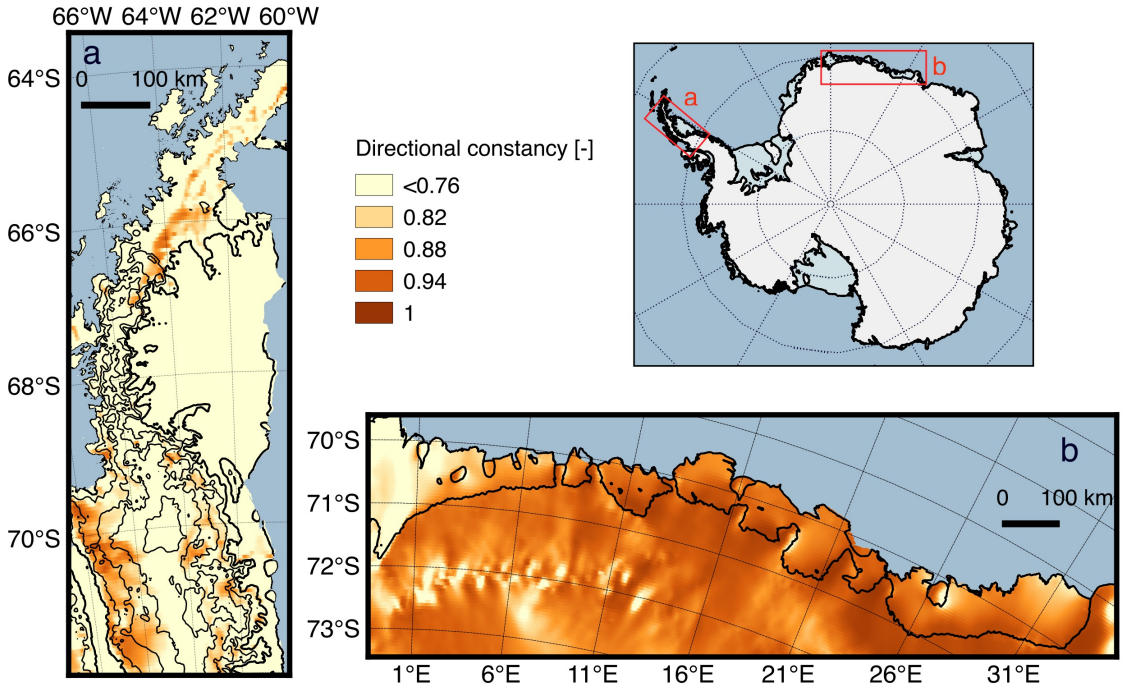

Supplementary Figure 2: Directional constancy of near-surface wind speed from RACMO2.3 around **(a)** the Larsen ice shelves in the Antarctic Peninsula [1] **(b)** and Dronning Maud Land.

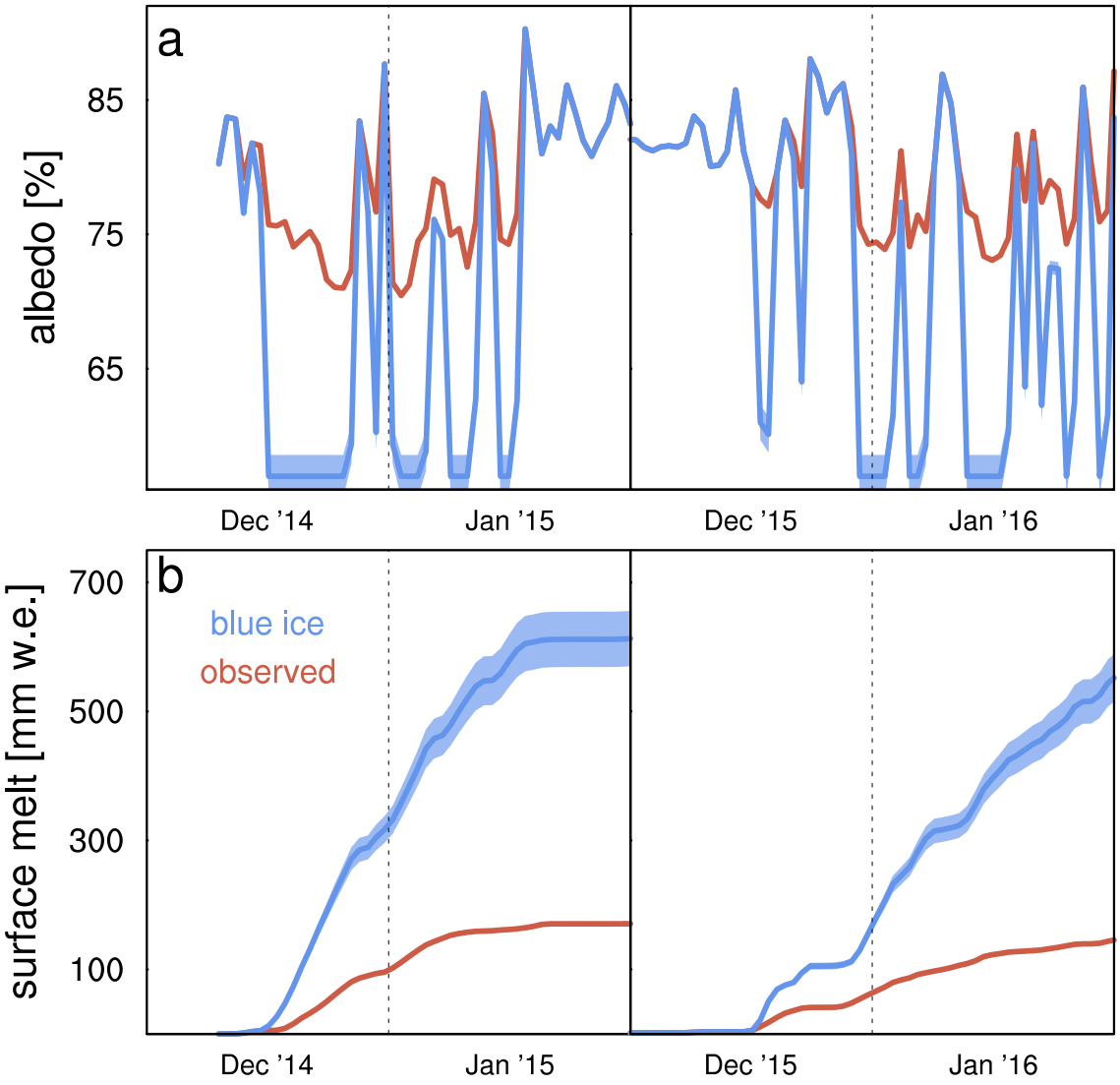

Supplementary Figure 3: **(a)** Albedo and **(b)** surface melt as calculated with the SEB model based on the iWS observations (red) and as derived by applying a blue-ice albedo (0.55-0.59 as derived by MODIS (see Methods, in blue)).

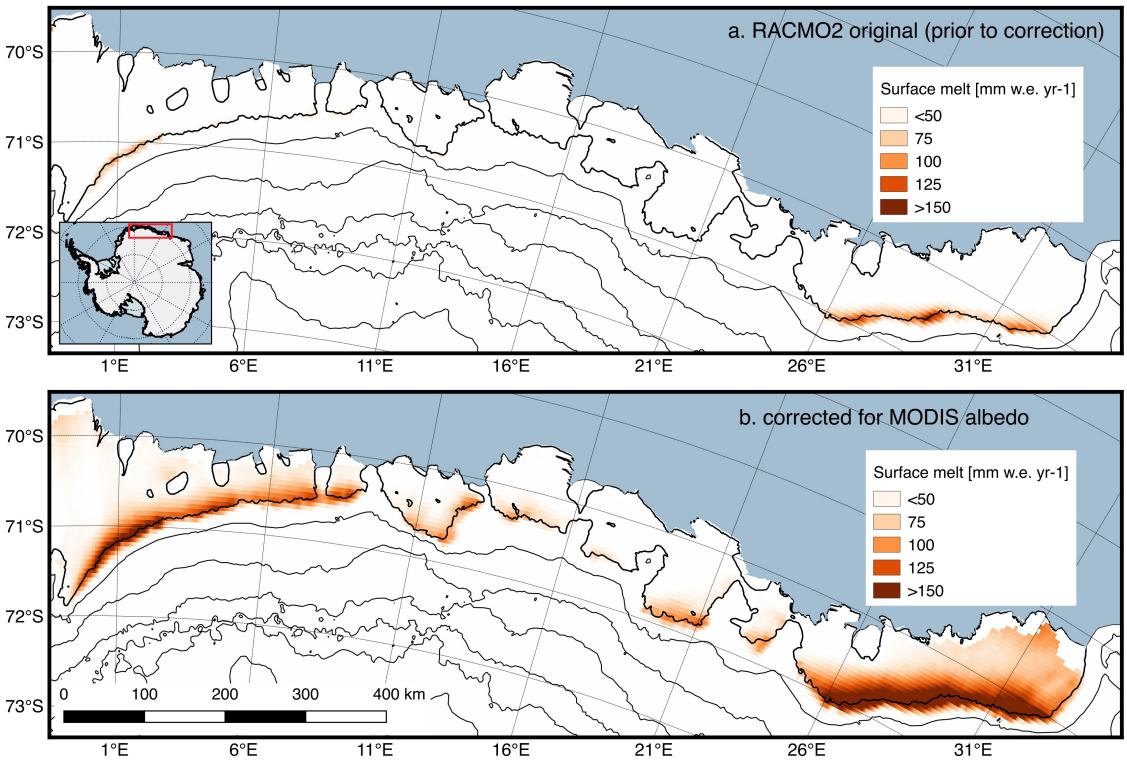

Supplementary Figure 4: Annual mean (1979-2015) surface melt in Dronning Maud Land simulated by RACMO2 **(a)** before correction and **(b)** after correction calculated using MODIS albedos (see Methods).

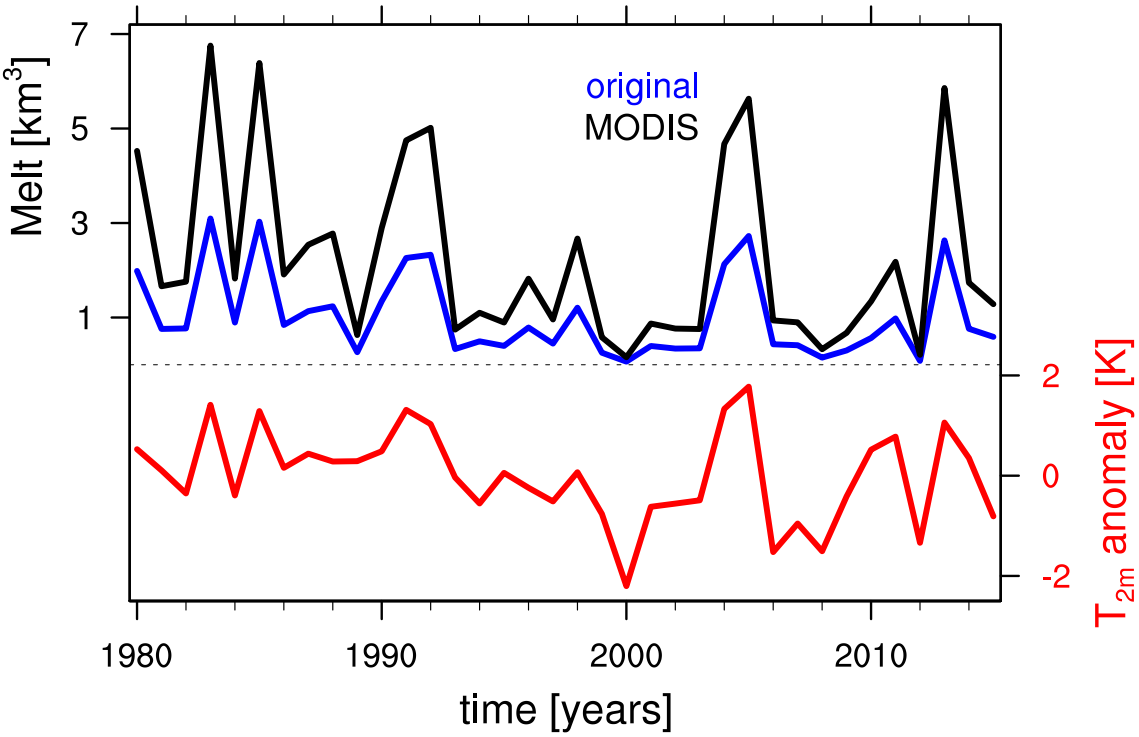

Supplementary Figure 5: Total summer RBIS grounding zone surface melt simulated by RACMO2.3 before (blue) and after correction using MODIS albedos (black, see Methods) and summer air temperature anomaly in the same region (red). Note that the year on the horizontal axis denotes the summer period starting in December in the prior year (e.g. 1980 refers to summer 1979-1980).

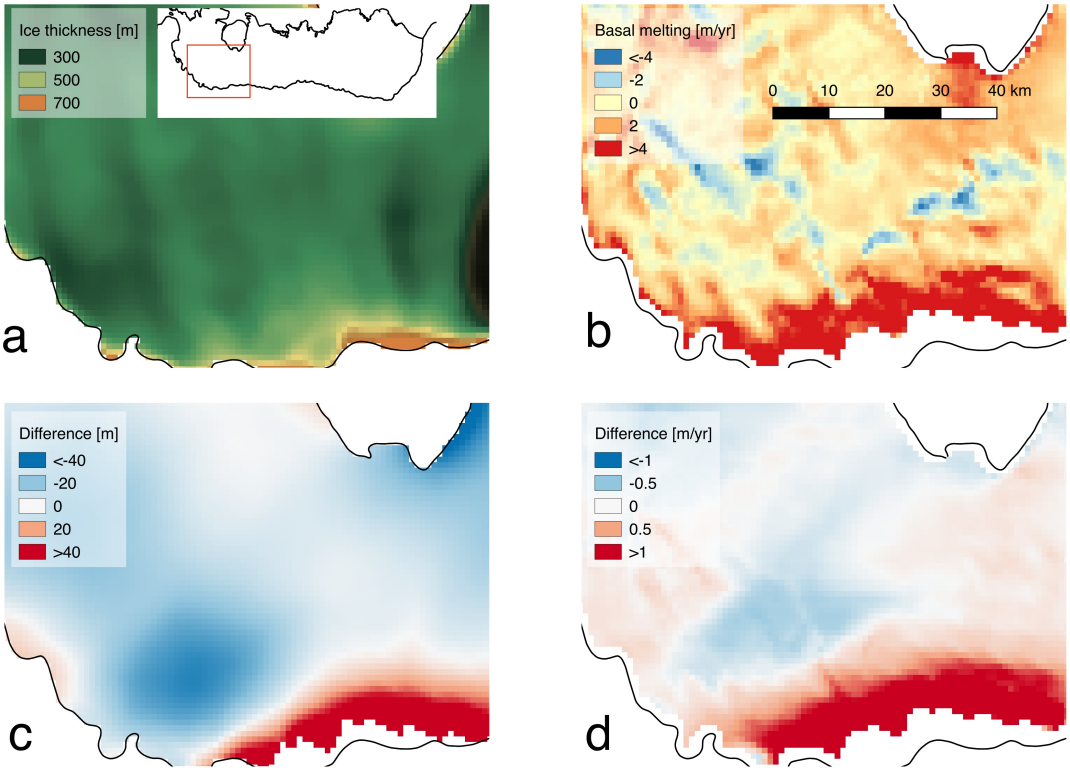

Supplementary Figure 6: **(a)** Ice thickness and **(b)** basal melt rates using the new FAC, surface elevation from Cryosat-2 [2], and observed ice fluxes at the grounding line [3]. **(b)** and **(b)** show the difference between results using the new, high-resolution RACMO2.3 output and the lower-resolution (27 km) RACMO2.3 output [4], the latter which only partly resolves the low FAC values in the RBIS grounding zone (new minus old). The ice thickness was derived assuming hydrostatic equilibrium from Cryosat-2 surface elevation, using the EIGEN-GL04C geoid [5] and an ice density of 910 $\mathrm{kg\,m^{-3}}$. Basal melt rates are derived from steady state mass conservation, using the thickness in (a) and observed ice velocities [6].

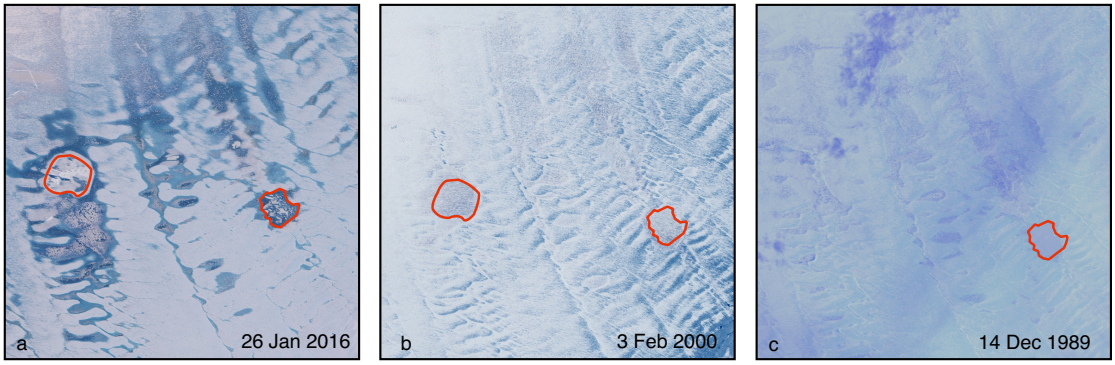

Supplementary Figure 7: Three LandSat scenes from summer of **(a)** 2015-2016, **(b)** 1999-2000, and **(c)** 1989-1990, for the eastern zoom region on RBIS (Figure 1). The two main meltwater features in 2016 (delineated in red) are also visible but displaced in 2000. In 1989, meltwater is visible at the surface, but the left-most doline is not clearly discernible, partly due to thin cloud cover and lower resolution imagery.

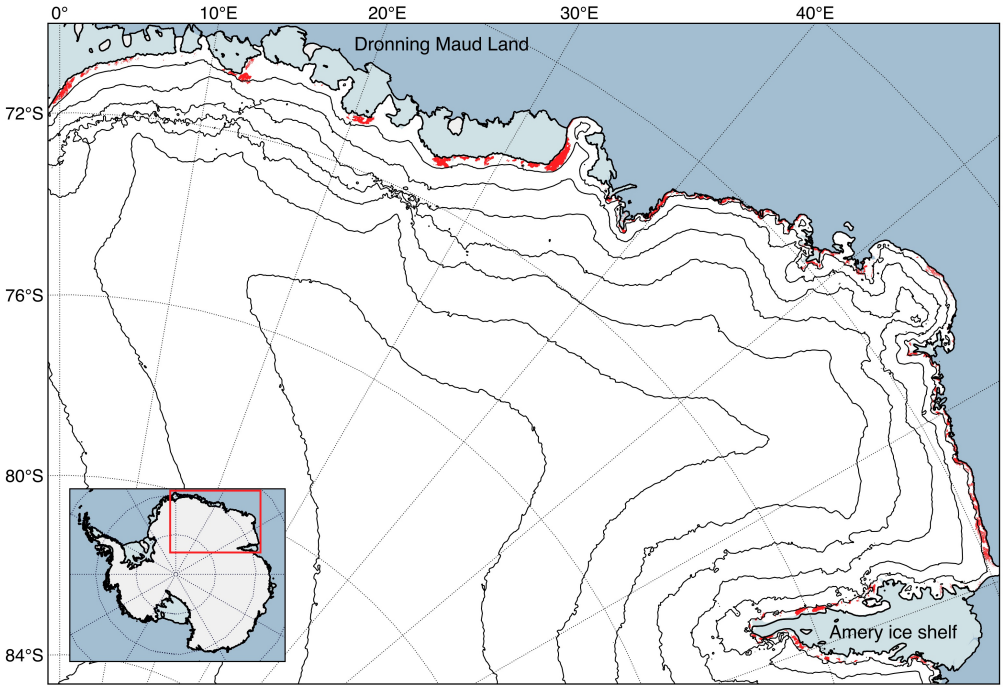

Supplementary Figure 8: Areas of intense wind-albedo interaction, i.e. overlap of high MWSD and blue ice or melting snow coverage below 500 m elevation (Figure 4) are shown in red over Dronning Maud Land and Amery ice shelf.

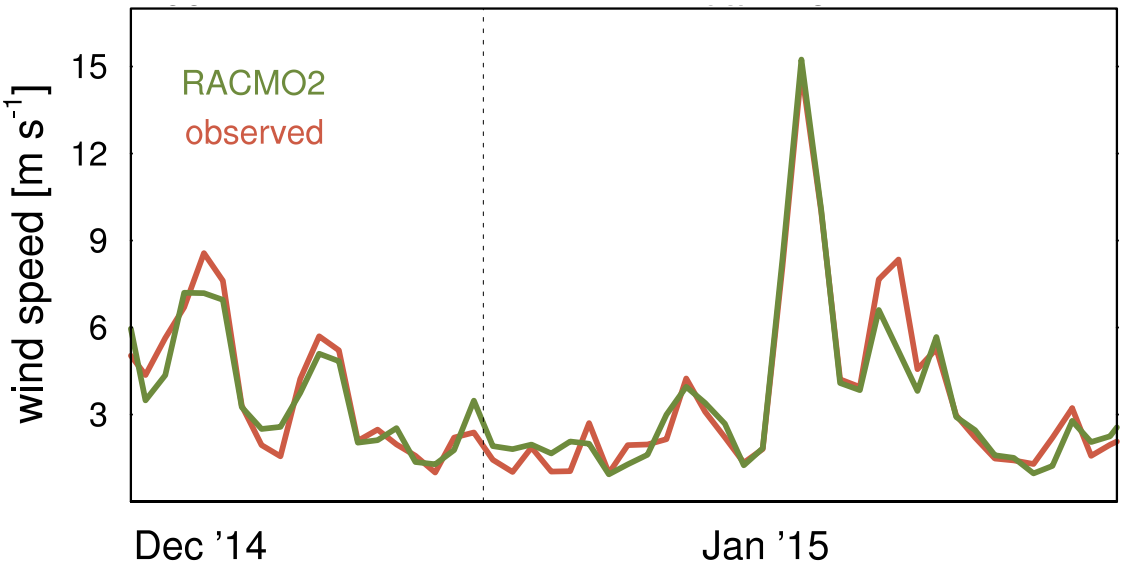

Supplementary Figure 9: Comparison of daily mean near-surface wind speed simulated by RACMO2 (green) and measured by the iWS (red) in summer 2014-2015.

References

[1] Van Wessem, J. M. *et al.* Temperature and wind climate of the Antarctic Peninsula as simulated by a high-resolution regional atmospheric climate model. *J. Clim.* **28**, 7306–7327 (2015).

[2] Helm, V., Humbert, A. & Miller, H. Elevation and elevation change of Greenland and Antarctica derived from CryoSat-2. *Cryosph.* **8**, 1539–1559 (2014).

[3] Depoorter, M. a. *et al.* Calving fluxes and basal melt rates of Antarctic ice shelves. *Nature* **502**, 89–92 (2013).

[4] Van Wessem, J. M. *et al.* Updated cloud physics in a regional atmospheric climate model improves the modelled surface energy balance of {Antarctica}. *Cryosph.* **8**, 125–135 (2014).

[5] Förste, C. *et al.* The GeoForschungsZentrum Potsdam/Groupe de Recherche de Géodésie Spatiale satellite-only and combined gravity field models: EIGEN-GL04S1 and EIGEN-GL04C. *J. Geod.* **82**, 331–346 (2008).

[6] Rignot, E., Mouginot, J. & Scheuchl, B. Ice Flow of the Antarctic Ice Sheet. *Science* **333**, 1427–1430 (2011).